Journal of Catalysis **189,** 1–15 (2000)
Article ID jcat.1999.2682, available online at http://www.idealibrary.com on IDEAL®

CO_2 Hydrogenation to Methanol on a $YBa_2Cu_3O_7$ Catalyst

L. Z. Gao and C. T. Au[1]

Chemistry Department and Center for Surface Analysis and Research, Hong Kong Baptist University, Kowloon Tong, Kowloon, Hong Kong, China

Received January 4, 1999; revised May 11, 1999; accepted September 13, 1999

The synthesis of methanol from CO_2 and H_2 over $YBa_2Cu_3O_7$ was studied. The aim was to clarify (i) the nature of the catalyst in the working state, (ii) the redox behaviour of copper in various oxidation states, and (iii) the formation and transformation of precursor species in methanol synthesis. The effects of reaction pressure, temperature, and space velocity on the catalytic performance were also investigated. The optimum reaction conditions were pressure = 3.0 MPa, space velocity = 3600 h^{-1}, and temperature = 240°C. After H_2 reduction at 250°C, the $YBa_2Cu_3O_7$ transformed from an orthorhombic to a tetragonal structure, a phase which is active for methanol synthesis. In a H_2-reduced $YBa_2Cu_3O_7$ sample, there were Cu^+ and oxygen vacancies and electrons trapped at the oxygen vacancies. We observed that CO_2 adsorption would consume the trapped electrons, resulting in the reoxidation of Cu^+ to Cu^{2+}. Intermediate species such as formate, methylenebisoxy, formyl, formaldehyde, and methoxide were observed in *in situ*-FTIR and FT-Raman studies; they were also captured by CD_3I during methanol synthesis. Based on these experimental results, a reaction mechanism for CO_2 hydrogenation to methanol over $YBa_2Cu_3O_7$ was proposed. In this mechanism, hydrogen adsorbs dissociatively at the Cu^+ sites of the CuO_x planes, whereas CO_2 adsorbs at the oxygen vacancies. The spillover of hydrogen atoms from Cu^+ to the oxygen atoms and/or carbon atom of adsorbed CO_2 leads to the formation of COOH, COHOH, HCOHOH, and H_2COHOH species; subsequently, one of the C–O bonds is weakened. Other intermediate species such as formate, methylenebisoxy, formyl, formaldehyde, and methoxide could be formed, and the final products are methanol, bimethyl ether, and CO.

Key Words: **$YBa_2Cu_3O_7$; methanol synthesis; CO_2 hydrogenation mechanism.**

1. INTRODUCTION

The synthesis of methanol over Cu/ZnO-type catalysts has been studied for years. However, several important questions remain unsolved. There are disagreements on (i) the working oxidation state of Cu, (ii) the roles of Cu and ZnO, (iii) the identity of the active sites, (iv) the structure of the catalyst, and (v) the reaction mechanism. ^{14}C labelling experiments under realistic industrial conditions (50 bar, 250°C) suggested that the carbon in methanol is mainly from CO_2 in a $CO/CO_2/H_2$ feed with a low CO_2/CO ratio (1–5). However, it is believed that CO hydrogenation could be significant at a higher temperature (6). Numerous workers have found that the ratio of CO_2/CO has clear effects on the rate of methanol formation (6–11). Klier and co-workers (12, 13) observed a maximum synthesis rate at $CO_2/CO = 1/14$. They claimed that, at lower CO_2 concentrations, the catalyst was deactivated due to overreduction by H_2 and CO, and at higher CO_2 concentrations, the synthesis was retarded due to the strong adsorption of CO_2. Lee and co-workers (11) found that an oxidized copper surface in a CO_2/H_2 feed was more active and stable than an overreduced one in a CO/H_2 feed. Carbon dioxide has been considered to have a role to play in controlling the surface composition, oxidation state, and dispersion of copper in the catalysts. It has been suggested that the predominant site for methanol synthesis is (i) metallic Cu (14, 15), (ii) Cu^+ species in close contact with ZnO (16, 17), (iii) Cu^0–Cu^+ couple (18), or (iv) the interface between Cu metal and the semiconductive ZnO support (19, 20).

Combined XRD/EXAFS spectra provided new insights into the structural changes during catalysis. Clausen *et al.* (21–23) found a reversible change in the apparent coordination number of the Cu atoms when the oxidation potential of the gas was changed. Specifically, it was observed that a significant increase in the coordination number for Cu occurred when the catalyst was exposed to a strongly oxidative gas. With a change back to a gas with lower oxidation potential, the coordination number decreased. The oxygen vacancies created in a reducing atmosphere may influence the structure and morphology of the catalyst, to which the catalytic activity is sensitive (24). Chinchen *et al.* (25, 26) proposed that the surface atomic oxygen O* plays important roles in methanol synthesis by promoting the adsorption of CO_2 and participating in the hydrogenation steps. This aroused extensive theoretical research on the bonding of atomic oxygen to copper crystals (e.g., 27, 28). However, such effects of surface O* could not be observed experimentally (29). Hydrogen spillover was proposed by Burch *et al.* (30). Most researchers considered formate species to be the intermediate in methanol synthesis (31–33). The formate species was also suggested to be an intermediate in

[1] To whom correspondence should be addressed. Fax: (852) 2339 7348. E-mail: pctau@hkbu.edu.hk.

0021-9517/00 $35.00

formic acid decomposition and in water–gas shift (WGS) reactions over Cu-containing catalysts (34–36).

The material $YBa_2Cu_3O_7$ is a well-known superconductor. The exceptionally wide range of oxygen nonstoichiometry and the high transport rate of oxygen make it a potentially attractive catalyst for oxidation. It has been used in oxidative reactions such as CO and light hydrocarbons oxidation to CO_2; CH_4 partial oxidation to CO, CH_3OH, CO_2, and HCHO (37); and toluene oxidation to benzonitrile (38). It can also be used as a catalyst for NO direct decomposition or NO reaction with CO to produce N_2 and CO_2 (39, 40). The catalytic activities are closely related to the nature of $YBa_2Cu_3O_7$, such as defined structure, the high and regular dispersion of copper, the oxygen vacancies, and the bivalent or trivalent states of copper. We envisage that it can also be employed as a model catalyst to study CO_2 and CO hydrogenations. In the present study, the hydrogenation of CO_2 on $YBa_2Cu_3O_7$ was reported. Temperature-programmed desorption (TPD), temperature-programmed surface reaction (TPSR), and pulse experiments were used to study CO_2 adsorption and transient reactions. Techniques such as XRD, TG/DTA, temperature-programmed reduction (TPR), EPR, and XPS were employed to investigate the structure, copper oxidation state, and redox ability of $YBa_2Cu_3O_7$. *In situ*-FTIR and laser FT-Raman spectroscopies were used to explore the reaction intermediates. Similar studies of CO hydrogenation on $YBa_2Cu_3O_7$ will be reported in a forthcoming paper.

2. EXPERIMENTAL

The $YBa_2Cu_3O_7$ sample was prepared by grinding stoichiometric amounts of high-purity nitrates of yttrium, barium, and copper. The mixture was heated in air at 600°C for 5 h. The material was then pressed, crushed, and sieved to 100–140 mesh and calcined at 900°C for 10 h. The BET surface area of the catalyst was determined by using nitrogen adsorption data at −196°C on a Nova 1200 system.

Methanol synthesis was conducted in a pressurized flow reactor. The reactor pressure was regulated by a back-pressure regulator. The catalytic performance was determined by placing 0.2 ml of catalyst into a microreactor connected to a gas manifold and operated with a feedstream containing a 3/1 mixture of H_2 and CO_2. The products were analyzed by means of GC. Prior to each experiment, the fresh catalyst was reduced *in situ* at 250°C for 8 h in a H_2/He (1/4) stream flowing at 60 ml min^{-1}.

Powder X-ray diffraction (XRD) studies were performed on a Rigaku D-Max Rotaflex diffractometer with Cu$K\alpha$ radiation and a Ni filter. X-ray diffraction data were collected at room temperature in the range of 5°–80°.

The H_2-TG/DTA measurements were carried out on a Rigaku thermoanalyzer. Fresh (nonreduced) sample (43 mg) was used. A mixture of 20% H_2–80% He (flow rate, 20 ml min^{-1}) was passed through the sample. The temperature range was from room temperature to 700°C and the heating rate was 10°C min^{-1}.

TPR was conducted by using a 10% H_2–90% N_2 (v/v) mixture. The flow rate of the carrier gas was 50 ml min^{-1} and a thermal conductivity detector was used. The amount of sample used was 0.2 g and the heating rate was 10°C min^{-1}. Before the TPR experiment was performed, the fresh sample was first calcined *in situ* at 800°C for 2 h under an oxygen flow of 15 ml min^{-1}, followed by cooling in oxygen to room temperature. The reduced (H_2, 250°C) or used sample was first treated *in situ* at 800°C for 2 h under a He flow of 15 ml min^{-1}, followed by being cooled in He to room temperature.

The dispersion of copper was determined on the basis of the measurement of N_2O decomposition at 90°C over the catalysts. The catalyst was reduced at 250°C in a mixture of 20% H_2–80% He for 8 h and purged with He for 2 h. The sample was then cooled down to 60°C. A quantity of N_2O was pulsed through the catalyst bed with He being the carrier gas. The surface concentration of Cu could be calculated according to the amount of N_2 produced.

EPR spectra were recorded at −196°C with a JEOL spectrometer operating in the X-band and calibrated with a DPPH standard ($g = 2.004$). The catalyst was placed in a self-made quartz cell in which the sample could be treated at various temperatures and atmospheres. For example, the sample could be treated in CO_2 (flow rate, 15 ml min^{-1}) at 250°C for 2 h, followed by being purged with He at the same temperature and then quenched in liquid nitrogen before EPR analysis.

Photoelectron spectra were recorded with a SKL-12 spectrometer equipped with a Mg$K\alpha$ X-ray source. The residual pressure in the analysis chamber was maintained below 10^{-9} Torr during data acquisition. The C(1*s*) peak at a binding energy of 284.6 eV was taken as an internal reference.

For TPD studies, the sample (0.2 g) was placed in the middle of a quartz microreactor with 4-mm i.d. The outlet gases were analyzed online by mass spectrometry (HP G1800A). The heating rate was 15°C min^{-1} and the temperature range was from room temperature to 800°C. Before the O_2-TPD experiments were performed, a fresh sample was heated in O_2 at 800°C for 2 h and then cooled to room temperature in O_2. For a reduced sample, the sample was H_2-reduced *in situ* at 250°C for 8 h, cooled to room temperature in He, and then heated in He from room temperature to 800°C for O_2-TPD study. Before the CO_2-TPD experiments were performed, a fresh sample was first calcined *in situ* at 800°C for 2 h under a flow of oxygen (20 ml min^{-1}) and then purged with helium to room temperature. For a reduced sample, it was first treated in helium for 2 h at 800°C and then cooled in He to room temperature. The CO_2-TPD experiment was performed according to the following procedures: the sample was kept in a flow of CO_2 (20 ml min^{-1}) for 1 h at a desired temperature and then cooled to room temperature

in CO_2. After being He-purged at room temperature for 1 h, the sample was heated to 800°C in helium.

TPSR experiments were carried out on a microreactor system. About 0.5 g of catalyst was packed in the middle of a quartz tube. The sample was exposed to CO_2 at a desired temperature for 2 h and then cooled to room temperature in CO_2, followed by He purging for 1 h. Then, the sample was heated to 700°C at a rate of 15°C min^{-1} under a H_2 flow. The outlet gases were analyzed by means of mass spectrometry.

Pulse reaction was carried out on a pulse microreactor system. Each pulse volume was 67.5 μl. During the reaction, H_2 was used as the carrier gas (flow rate, 20 ml min^{-1}).

A chemical-trapping experiment was performed during TPSR and CO_2-pulsing experiments by injecting CD_3I (0.2 μl) onto the sample. The products were analyzed by mass spectrometry.

In situ-FTIR spectra were collected on a Nicolet series II magna-IR 550 spectrometer with a SPECTRA TECH *in situ* cell. The catalyst powder weighing approximately 70 mg was contained in a low-dead volume infrared cell. The cell was heated by means of an electrical resistance heater. *In situ*-absorbance spectra were obtained at 4-cm^{-1} resolution. The spectra were then referenced to a spectrum of the catalyst collected at the same temperature under a He or H_2 flow, as appropriate. Before FTIR spectrum collection, the cell was pumped for 5 min to remove gaseous CO_2 and H_2.

Laser FT-Raman spectra were recorded using a Nicolet 560 FT-Raman spectrometer with a He–Ne laser operating at a power of 1 mW. Spectra were collected at a resolution of 4 cm^{-1}. The sample (0.1 g) in a self-made quartz tube could be heated to 800°C and exposed to reactant gas without exposure to air.

3. RESULTS

3.1. Catalytic Activities

We observed that a reduced (H_2, 250°C) $YBa_2Cu_3O_7$ catalyst was active in CO_2 hydrogenation whereas a fresh (nonreduced) one was not. Tables 1–3 show the effects of reaction temperature, pressure, and space velocity on the catalytic performance. One can observe that the products of CO_2 hydrogenation over the catalyst are CO, CH_3OCH_3, and CH_3OH. High pressure, high space velocity, and low temperature are favourable to methanol and CH_3OCH_3 formations, whereas the opposite is true for CO formation. High pressure, high temperature, and low space velocity are favourable to CO_2 conversion. The reaction competitive to methanol synthesis is the RWGS (reverse water–gas shift) reaction. The BET surface area of the catalyst was 4.5 m^2 g^{-1}.

TABLE 1

Effects of Reaction Temperature on the Catalytic Performance

Reaction temperature (°C)	CO_2 conversion (%)	Rate of CO_2 reaction (10^{-3} mol m^{-2} h^{-1})	Products selectivity (%)		
			MeOH	DME	CO
200	0.9	1.1	72.5	5.8	20.1
220	1.2	1.4	71.3	5.5	23.2
240	3.4	3.8	50.7	3.4	45.9
260	4.4	4.8	34.8	2.5	62.7
280	4.6	4.8	30.6	2.1	63.4

Note. MeOH: methanol; DME: dimethyl ether. Reaction conditions: pressure = 3.0 MPa; GHSV = 3600 h^{-1}; $H_2/CO_2 = 3:1$ (molar ratio).

TABLE 2

Effects of Space Velocity on the Catalytic Performance

Space velocity (h^{-1})	CO_2 conversion (%)	Rate of CO_2 reaction (10^{-3} mol m^{-2} h^{-1})	Products selectivity (%)		
			MeOH	DME	CO
1800	4.2	2.4	34.9	2.6	62.5
3600	3.0	3.4	38.4	3.3	58.3
5400	2.7	4.6	44.2	3.7	52.1
7200	1.8	4.1	48.9	4.1	47.0
9000	1.4	3.9	51.1	4.1	44.8

Note. MeOH: methanol; DME: dimethyl ether. Reaction conditions: pressure = 3.0 MPa; T = 240°C; $H_2/CO_2 = 3:1$ (molar ratio).

3.2. XRD, H_2 TG/DTA, and TPR

The XRD pattern of a fresh sample indicated that the material was single-phase and was orthorhombic in structure. It can be formulated as $YBa_2Cu_3O_7$ (41). After reduction in H_2 at 250°C, it transformed to a tetragonal structure with the composition of $YBa_2Cu_3O_6$. There are Cu^{2+} and Cu^{3+} in $YBa_2Cu_3O_7$ (42), whereas there are Cu^{+} and Cu^{2+} in $YBa_2Cu_3O_6$ (43). There should be oxygen vacancies generated in the lattice of tetragonal $YBa_2Cu_3O_6$. Figure 1A shows the H_2-TG/DTA curves of $YBa_2Cu_3O_7$. There are two weight loss steps in the TG curve at ca. 240 and 420°C; the former is corresponding to an exothermic effect whereas the latter is to an endothermic effect. The transformation of phase from orthorhombic to tetragonal takes place at ca. 240°C. After reduction at 400°C, we found that the $YBa_2Cu_3O_6$ sample was broken down

TABLE 3

Effects of Reaction Pressure on the Catalytic Performance

Reaction pressure (Mpa)	CO_2 conversion (%)	Rate of CO_2 reaction (10^{-3} mol m^{-2} h^{-1})	Products selectivity (%)		
			MeOH	DME	CO
0.5	2.0	0.4	12.1	0.8	87.4
1.0	2.7	1.0	27.6	3.2	69.2
2.0	3.0	2.3	38.4	3.3	58.3
3.0	3.4	3.8	50.7	3.4	45.9

Note. MeOH: methanol; DME: dimethyl ether. Reaction conditions: $T = 240$°C; GHSV = 3600 h^{-1}; $H_2/CO_2 = 3:1$ (molar ratio).

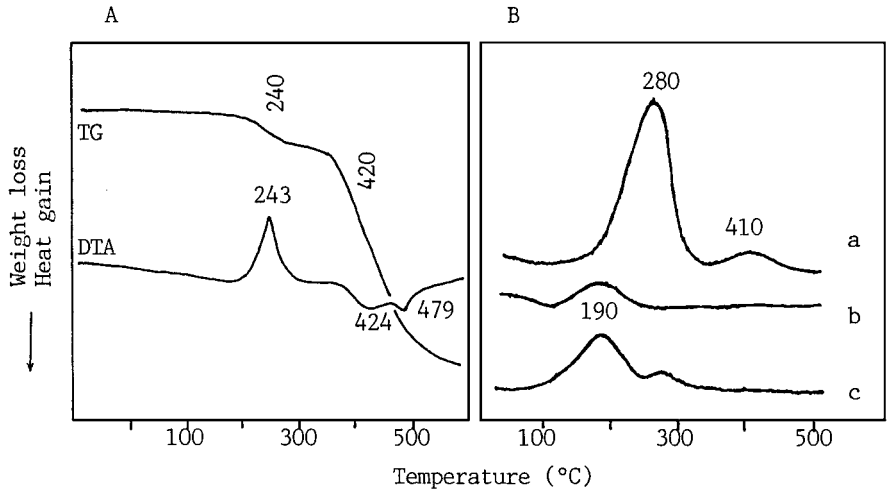

FIG. 1. (A) H_2-TG/DTA profiles for fresh $YBa_2Cu_3O_7$. (B) TPR curves for (a) fresh $YBa_2Cu_3O_7$, (b) reduced (H_2, 250°C) $YBa_2Cu_3O_7$, and (c) reduced (H_2, 250°C) $YBa_2Cu_3O_7$ used for CO_2 hydrogenation.

to a mixture of CuO, Cu_2O, Cu, BaO, and Y_2O_3. Depending on the weight loss, the composition during reduction at 250°C was approximately $YBa_2Cu_3O_{6.325}$, which could also be speculated as $YBa_2Cu^{2+}{}_{2.65}Cu^{+}{}_{0.35}O_{6.325}$ or $YBa_2Cu^{0}{}_{0.175}Cu^{2+}{}_{2.825}O_{6.325}$.

Figure 1B shows the TPR profiles of fresh $YBa_2Cu_3O_7$, reduced (H_2, 250°C) $YBa_2Cu_3O_7$, and $YBa_2Cu_3O_7$ used for CO_2 hydrogenation. In profile 1B(a), there are a strong peak centered at ca. 280°C and a weak one at ca. 410°C. The former corresponds to the first weight loss and the latter to the second weight loss in the TG curve (Fig. 1A). Profile 1B(b) shows only one small peak at ca. 190°C, implying that after reduction at 250°C $YBa_2Cu_3O_{6.325}$ could still be reduced slightly at ca. 190°C and become $YBa_2Cu_3O_{6.325-y}$. This also means that the potential of oxygen mobility in tetragonal $YBa_2Cu_3O_{6.325}$ is higher than that in $YBa_2Cu_3O_7$, while the content of mobile oxygen in $YBa_2Cu_3O_{6.325}$ is less than that in $YBa_2Cu_3O_7$. Profile 1B(c) is the TPR profile of $YBa_2Cu_3O_7$ used in a CO_2 hydrogenation reaction. A strong reduction band at 190°C and a weak one at 280°C were observed, indicating that after CO_2 hydrogenation the reduced catalyst was somewhat reoxidized.

3.3. N_2O Titration

The concentration of surface Cu^0 could be estimated according to the stoichiometric reaction of N_2O with metallic Cu at 90°C (44, 45):

$$N_2O + 2Cu \rightarrow N_2 + Cu_2O. \qquad [1]$$

However, the titration with N_2O at 90°C of a $YBa_2Cu_3O_7$ sample H_2-reduced at 250°C showed no N_2 formation. The result suggests that there was no metallic copper on the reduced sample. For a $YBa_2Cu_3O_7$ sample H_2-reduced at 400°C, N_2O titration at 90°C produced N_2.

3.4. EPR and XPS

The EPR spectrum of a fresh $YBa_2Cu_3O_7$ sample depicted in Fig. 2a exhibits a strong anisotropic signal with extremes at $g_1 = 2.231$, $g_2 = 2.130$, and $g_3 = 2.053$, which are typical features of Cu^{2+} (46, 47). The broad line and the unresolved hyperfine structure are due to interaction among the Cu^{2+} species: the signal is broadened by magnetic dipolar interactions (and possibly, some spin exchange) between neighbouring paramagnetic ions. When $YBa_2Cu_3O_7$ was heated at 800°C in He, a signal centered at $g = 2.005$ (Fig. 2b) appeared, which could be attributed to e^- formed at the sites of surface oxygen vacancies in $YBa_2Cu_3O_7$ according to the mechanism

$$O^{2-} \rightarrow 1/2O_2 \text{ (desorbed)} + 2[e^-], \qquad [2]$$

in which [ ] represents oxygen vacancies.

Figure 2c shows the EPR spectrum of $YBa_2Cu_3O_7$ after the sample was reduced in H_2 at 250°C. One can observe that the intensity of the Cu^{2+} signal decreased dramatically after reduction, indicating the partial reduction of Cu^{2+} to Cu^+. The e^- signal at ca. $g = 2.005$ was generated due to the reactions

$$H_2 \rightarrow 2H, \qquad [3]$$

$$H + O^{2-} \rightarrow HO^- + [e^-]. \qquad [4]$$

The electrons, e^-, were located at the oxygen vacancies and can reduce Cu^{2+} to Cu^+:

$$Cu^{2+} + [e^-] \rightarrow Cu^+ + [\,]. \qquad [5]$$

The EPR features of Cu^{2+} were almost unchanged when CO_2 was adsorbed on a nonreduced $YBa_2Cu_3O_7$ sample

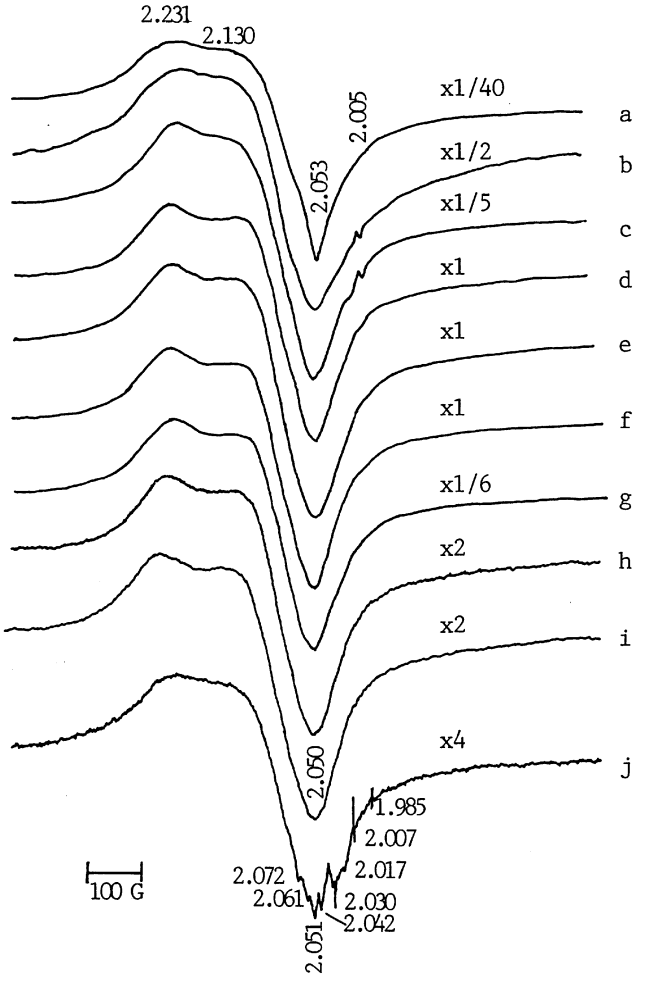

FIG. 2. EPR spectra of (a) fresh $YBa_2Cu_3O_7$, (b) $YBa_2Cu_3O_7$ heated at 800°C in He, (c) reduced (H_2, 250°C) $YBa_2Cu_3O_7$, reduced (H_2, 250°C) $YBa_2Cu_3O_7$ sample exposed to (d) CO_2 at 250°C, (e) CO_2 at 300°C, (f) CO_2/H_2 (3/1) at 250°C, (g) CO_2/H_2 (1/1) at 250°C, (h) CO_2/H_2 (1/3) at 250°C, CO_2/H_2 (1/4) at 250°C, and (j) NO at 250°C.

at various temperatures. The Cu^{2+} signal did not change in intensity either. However, CO_2 adsorption at 250 and 300°C on a reduced $YBa_2Cu_3O_7$ sample would cause the e^- signal at ca. 2.005 to diminish (Figs. 2d and 2e), resulting in the oxidation of Cu^+ and formation of CO_2^-, i.e.,

$$Cu^+ \rightarrow e^- + Cu^{2+}, \quad [6]$$

$$CO_2 + e^- \rightarrow CO_2^-. \quad [7]$$

Mill *et al.* (48) and Solymosi *et al.* (49) reported that the adsorption of CO_2 on a cesium/silica surface and a K-modified Rh/SiO_2 surface would result in the formation of CO_2^-.

Figures 2f–2i illustrated the EPR spectra after the reduced $YBa_2Cu_3O_7$ sample was exposed to a mixture of CO_2/H_2 with molar ratios of 3/1, 1/1, 1/3, or 1/4, respectively. The e^- signal disappeared in all the four spectra, implying that under a CO_2- or H_2-rich circumstance, the trapped electrons can be consumed and redox reactions such as reactions [5] and [6] could have taken place in a CO_2/H_2 atmosphere.

As we did not observe any 2100-G isotropic hyperfine splitting of Cu^0 atoms, we can be sure that there was no metallic copper in the sample (50). The adsorption of NO on a reduced $YBa_2Cu_3O_7$ sample would result in a EPR spectrum in which one can observe Cu^+–NO species (Fig. 2j). This proves that Cu^+ existed (51, 52). Arakawa and Adachi suggested that the Cu^{2+} and Cu^+ ions adjacent to the oxygen vacancies in $YBa_2Cu_3O_{7-\delta}$ functioned as the active centers for the activation of NO (53). Comparison of the EPR spectrum of reduced $YBa_2Cu_3O_7$ to the EPR spectrum of a reduced $YBa_2Cu_3O_7$ sample exposed to N_2O at 90°C showed no feature modification; this demonstrates that there were no Cu^0 atoms in the reduced sample and reaction [1] did not happen.

The XPS lines of the Cu($2p_{3/2}$) level of a $YBa_2Cu_3O_7$ sample after various treatments are shown in Fig. 3. The fresh $YBa_2Cu_3O_7$ sample shows one peak with B.E. = 933.9 eV

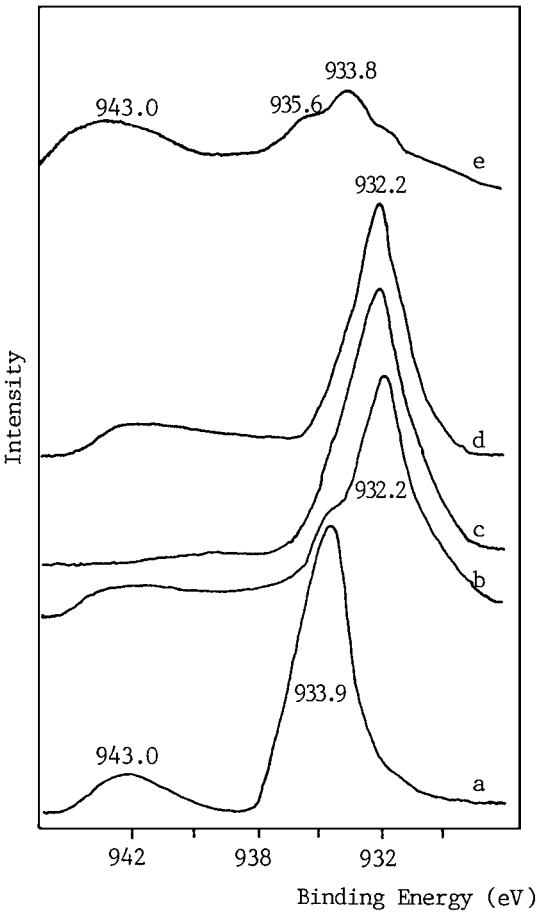

FIG. 3. Cu($2p_{3/2}$) XPS spectra of (a) fresh $YBa_2Cu_3O_7$, (b) reduced (H_2, 250°C) $YBa_2Cu_3O_7$, (c) reduced (H_2, 400°C) $YBa_2Cu_3O_7$, (d) reduced (H_2, 250°C) $YBa_2Cu_3O_7$ exposed to CO_2/H_2 (1/3) at 250°C, and (e) reduced (H_2, 250°C) $YBa_2Cu_3O_7$ after CO_2 TPD.

(Fig. 3a), which corresponds to Cu^{2+}. A satellite peak at 943.0 eV, which is a characteristic feature of Cu^{2+}, was also observed. After reduction at 250°C, the Cu($2p_{3/2}$) XPS spectrum shows a weak shoulder at B.E. = 933.9 eV and a strong peak at 932.2 eV which could be assigned to Cu^{+} or Cu^{0} (Fig. 3b). Together with the 933.9-eV peak, the satellite peak corresponding to Cu^{2+} reduced in intensity. After further reduction at 400°C, only the peak at 932.2 eV remained (Fig. 3c). Exposure of a sample reduced at 250°C to a reaction mixture of CO_2 and H_2 at 250°C could also result in a peak at 932.2 eV (Fig. 3d). After the adsorption and desorption of CO_2 in a CO_2-TPD study, a profile with three components at ca. 935.6, 933.8, and 932.2 eV, and a satellite peak at 943.0 eV was observed. The highest peak intensity was at ca. 933.8 eV (Fig. 3e), indicating that CO_2 can oxidize Cu^{+} to Cu^{2+}. Usually, the signal at B.E. = 935.6 eV is assigned to tetrahedrally coordinated Cu^{2+} sites while that at about 933.8 eV is assigned to octahedrally coordinated Cu^{2+} sites (54, 55). The distinction between the Cu^{+} and Cu^{0} cannot be confirmed solely on the basis of the B.E. of the Cu($2p_{3/2}$) level (56). We had turned to the X-ray-induced Cu LMM Auger line for final confirmation. After reduction, the Auger profile of a fresh $YBa_2Cu_3O_7$ sample changed from a broad peak centered at 918.0 eV (K.E.) to a strong peak centered at 917.2 eV (K.E.) with two shoulders at 918.1 eV (K.E.) and 918.6 eV (K.E.). According to the approach of Okamoto *et al.* (56), we concluded that it was Cu^{+} rather than Cu^{0} that existed on the surface of $YBa_2Cu_3O_7$ after H_2 reduction at 250°C.

3.5. O_2 TPD

Figure 4 shows the O_2-TPD profiles of fresh $YBa_2Cu_3O_7$ and reduced $YBa_2Cu_3O_7$. For a fresh $YBa_2Cu_3O_7$ sample, there was large O_2 desorption starting at ca. 600°C (Fig. 4a). Somorjai (57) reported that some oxides could be reduced slightly due to O_2 desorption at high temperatures in vacuum. No apparent O_2 desorption was observed over a reduced $YBa_2Cu_3O_7$ sample (Fig. 4b), but H_2O ($m/z = 18$) intensity increased with temperature rise (Fig. 4c). These indicate that, after reduction, there were H atoms left in the catalyst, which reacted with oxygen to give water.

3.6. CO_2 TPD

The CO_2-TPD profiles of a fresh $YBa_2Cu_3O_7$ sample exposed to CO_2 at 200, 250, or 350°C are shown in Fig. 5A. According to the profile of desorption for CO_2 adsorption at 200°C (Fig. 5A(a)), there could be three types of basic sites on the $YBa_2Cu_3O_7$ sample: CO_2 desorptions at the ranges of (i) <300°C, (ii) 300–500°C, and (iii) >600°C. The desorption of CO_2 above 600°C is attributed to carbonates decomposition. The CO_2-TPD profiles of a reduced (H_2, 250°C) $YBa_2Cu_3O_7$ sample exposed to CO_2 at 200, 250, 300, or 400°C (Fig. 5B) exhibited very different features relative

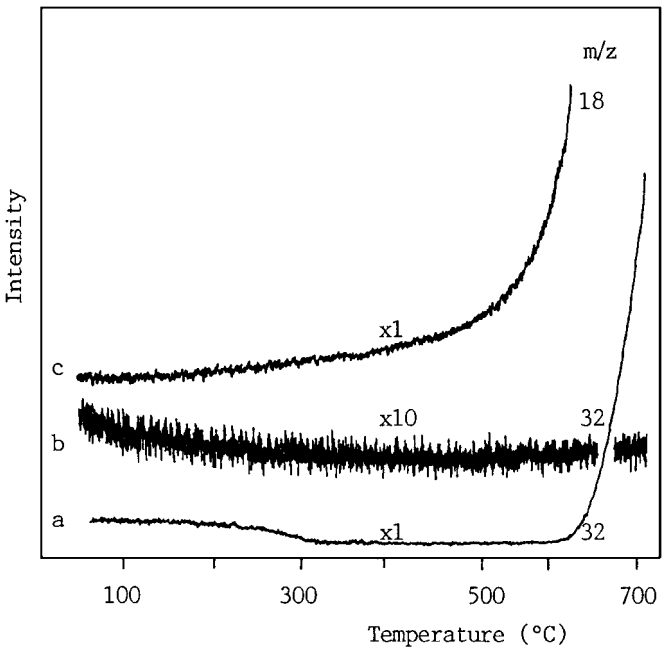

FIG. 4. O_2 ($m/z = 32$) desorption over (a) fresh $YBa_2Cu_3O_7$ and (b) reduced (H_2, 250°C) $YBa_2Cu_3O_7$; (c) H_2O ($m/z = 18$) desorption on reduced (H_2, 250°C) $YBa_2Cu_3O_7$ during O_2-TPD performance.

to those of a fresh $YBa_2Cu_3O_7$ sample. There was only one CO_2 desorption peak, implying that there was only one kind of basic site on the reduced $YBa_2Cu_3O_7$ sample. The desorption temperatures were 227, 280, 340, and 420°C (peak area was in turn increased) for CO_2 adsorptions at 200, 250, 300, and 400°C, respectively. Comparing to the CO_2-TPD profile of a nonreduced $YBa_2Cu_3O_7$ sample, the obvious difference is that there was no CO_2 desorption at temperatures above 600°C, indicating that there was no carbonate formation when CO_2 adsorbed on a reduced $YBa_2Cu_3O_7$ sample.

3.7. CO_2 TPSR

The CO_2-TPSR experiment was performed with a sample exposed (at 250°C) to CO_2 being heated in a flow of H_2. The spectra are shown in Fig. 6. There were CO_2 desorptions at ca. 80, 150, 200, 330, and above 620°C. Comparing to the results in Fig. 5B, we found that the intensity of CO_2 desorption at around 320°C was very low and there was still a little CO_2 desorption above 600°C, indicating that there was carbonate or bicarbonate formation when H_2 reacted with the adsorbed CO_2. We observed that there were CO and H_2O desorptions above ca. 600°C, an indication of the occurrence of the RWGS reaction. In the CD_3I trapping experiments, CD_3COOH ($m/z = 63$) and CD_3OCH_3 ($m/z = 49$) were detected from 80 to 360°C, whereas CD_3CHO ($m/z = 47$) was detected only above 260°C during TPSR experiments. These imply

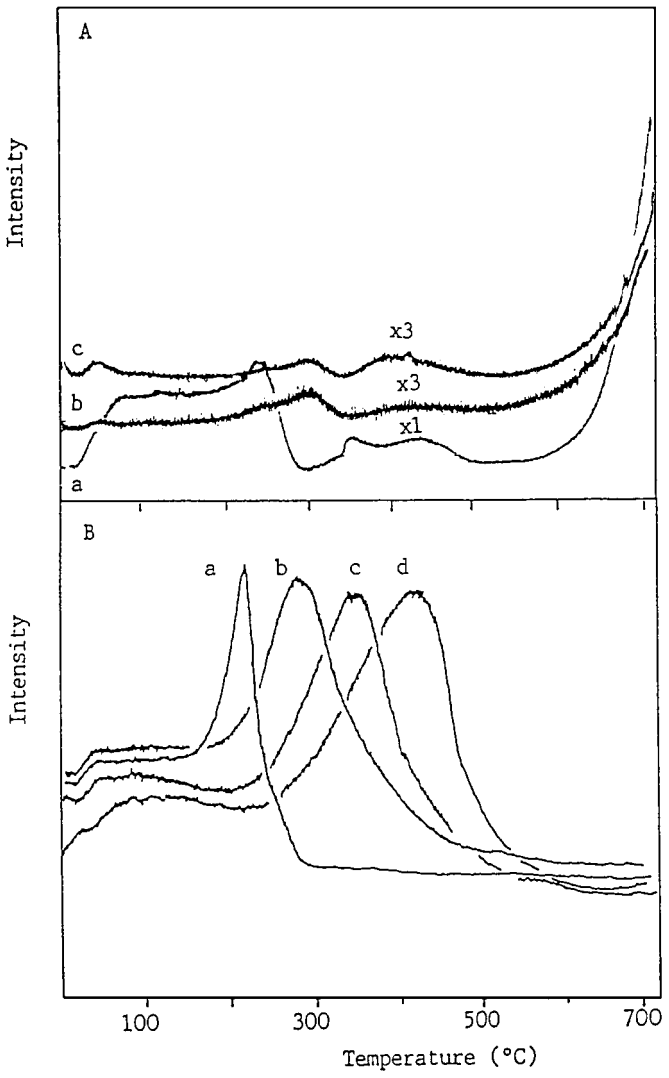

FIG. 5. (A) CO_2-TPD profiles over fresh $YBa_2Cu_3O_7$ with CO_2 adsorbed at (a) 200°C, (b) 250°C, and (c) 350°C. (B) CO_2-TPD profiles over reduced (H_2, 250°C) $YBa_2Cu_3O_7$ with CO_2 adsorbed at (a) 200°C, (b) 250°C, (c) 300°C, and (d) 400°C.

that formyl, formate, and methoxy were generated in CO_2 hydrogenation and formate generation was more feasible than formyl production.

3.8. Pulse Studies

MS spectra of CO_2 pulse studies at 250°C over the reduced (H_2, 250°C) $YBa_2Cu_3O_7$ sample with H_2 as the carrier gas are shown in Fig. 7. There was almost no CO_2 detection for the first three CO_2 pulses, indicating that most of the CO_2 molecules were adsorbed on the catalyst and were difficult to desorb. At the 11th pulse, the peak area of CO_2 reached the highest value. When CD_3I was injected during CO_2 pulsing in H_2, we detected CD_3OCH_3 and CD_3COOH. The result indicates that formate and methoxide were generated during CO_2 hydrogenation.

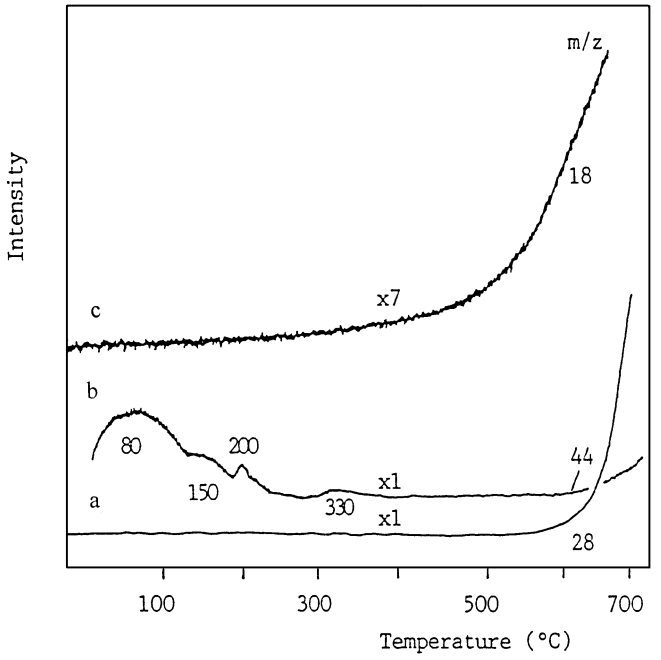

FIG. 6. Desorption of species with m/z = (a) 28 (CO), (b) 44 (CO_2), and (c) 18 (H_2O) during TPSR (CO_2, H_2) performed on reduced (H_2, 250°C) $YBa_2Cu_3O_7$.

3.9. In Situ FTIR

3.9.1. Fresh $YBa_2Cu_3O_7$ and reduced $YBa_2Cu_3O_7$. Figure 8 shows the *in situ*-FTIR spectra of the fresh and reduced (H_2, 250°C) $YBa_2Cu_3O_7$ samples. After reduction, the OH^- band at ca. 3500 cm^{-1} increased in intensity (Fig. 8b). The absorption bands at 677, 556, and 430 cm^{-1} are due to in-plane oxygen motion, out-of-plane Cu motion, and out-of-plane oxygen motion, respectively (58a). One should take into consideration that the stretching of Cu–O–Cu in a tetragonal phase is somewhat different from that in an orthorhombic phase. Both $YBa_2Cu_3O_7$ and La_2CuO_4 have perovskite-related structures. In La_2CuO_4, if metallic copper existed, the in-plane mode response at 677 cm^{-1} would be completely shielded (58a). In Figs. 8a and 8b, the

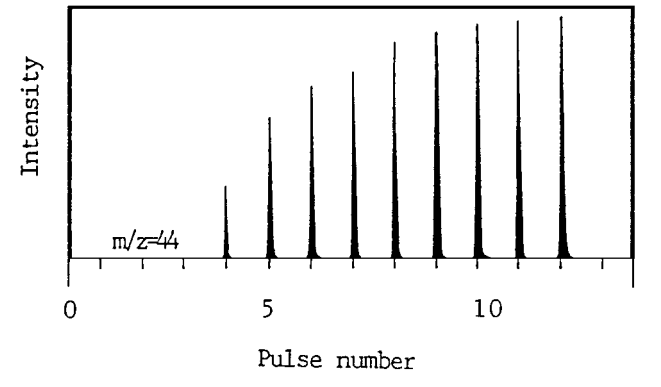

FIG. 7. Transient response of species with $m/z = 44$ (CO_2) during CO_2 pulsing on reduced (H_2, 250°C) $YBa_2Cu_3O_7$ with H_2 being the carrier gas.

bands at 677 cm^{-1} are not shielded; we suggest that there was no metallic copper atom in both the fresh and reduced $YBa_2Cu_3O_7$ samples.

3.9.2. CO_2 and H_2 adsorptions on fresh $YBa_2Cu_3O_7$. Based on the interpretations in Refs. 33, 48, 49, and 58b–66, IR bands are assigned to various species as indicated in Table 4. The FTIR spectrum for H_2/CO_2 (3:1, 3.0 MPa) adsorbed on a fresh $YBa_2Cu_3O_7$ sample at 250°C was recorded as shown in Fig. 9a. The bands attributable to ionic (1450 cm^{-1}), bidentate carbonates (1563 cm^{-1}), and bidentate bicarbonates (1610 cm^{-1}) species were detected.

3.9.3. CO_2 and H_2 adsorptions on reduced $YBa_2Cu_3O_7$. Figure 9b shows the FTIR spectrum obtained by flowing CO_2 over a reduced (H_2, 250°C) $YBa_2Cu_3O_7$ sample at 250°C and at 3.0 MPa for 0.5 h. The bands attributable to ionic, bidentate carbonates, monodentate (1360 cm^{-1}) and bidentate (1535, 2849, 2922 cm^{-1}) formates, hydroxide (3361 cm^{-1}), bidentate methylenebisoxy (2970, 2868 cm^{-1}), CO_2^- anion species (1325, 1695 cm^{-1}), and C–O–C stretching (915, 1060 cm^{-1}) were observed. With the rise in CO_2 adsorption temperature to 350°C, bands attributable to methyl formate (1658, 1731 cm^{-1}), ionic carbonate, CO_2^-, and hydroxide were observed; the bands due to bidentate formate and bidentate methylenebisoxy were dramatically weakened. Nevertheless, a broad band with weak intensity attributable to $CO–Cu^+$ (2130 cm^{-1}) was detected (Fig. 9c). The FTIR spectrum presented in Fig. 9d shows that after H_2/CO_2 (3:1, 3.0 MPa) adsorption at 250°C, the bands ascribed to bidentate formate, methoxide (2957 cm^{-1}), methylenebisoxy, formyl and formaldehyde (1763, 2707, 2880 cm^{-1}), CO_2^-, and C–O–C stretching were clearly observed.

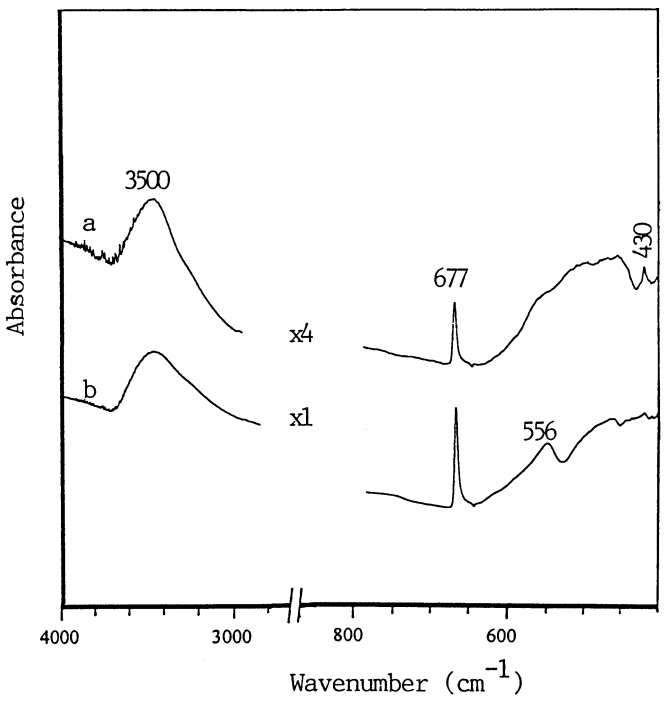

FIG. 8. Infrared spectra of (a) fresh $YBa_2Cu_3O_7$ and (b) reduced (H_2, 250°C) $YBa_2Cu_3O_7$.

TABLE 4

Assignments of FTIR Absorbance Bands

Wavenumber (cm^{-1})	Assignment	References
1605	$H_2O_{(a)}$	33
1450	*i*-$CO_{3(a)}$ (ionic carbonate)	59
1371, 1461	*m*-$CO_{3(a)}$ (monodentate carbonate)	59
1405	*p*-$CO_{3(a)}$ (polydentate carbonate)	59, 60
1563	*b*-$CO_{3(a)}$ (bidentate carbonate)	60
1610	*b*-$HCO_{3(a)}$ (bidentate bicarbonate)	60
1535, 2849, 2922	*b*-$HCOO_{(a)}$ (bidentate formate)	61, 60
1360	*m*-$HCOO_{(a)}$ (monodentate formate)	61, 60
2957	$CH_3O_{(a)}$ (methoxide)	64, 33
2970, 2868	*b*-$CH_2OO_{(a)}$ (bidentate methylenebisoxy)	62
3361	$OH_{(a)}$ (hydroxide)	33
1730, 2707, 2880	$CH_2O_{(a)}$ (formaldehyde), $HCO_{(a)}$ (formyl)	33, 66
1658, 1731	$CH_3OCHO_{(a)}$ (methyl formate)	64, 65
1695	CO_2^- (antisymmetric stretch)	48, 49
1325	CO_2^- (symmetric stretch)	48, 49
2130	$CO_{(a)}–Cu^+$ (linear adsorbed CO on Cu^+)	63
2077	$CO_{(a)}$–Cu (linear adsorbed CO on Cu^0)	63
915, 1060	C–O–C (stretch)	58(b), 66

Note. (a) means adsorbed.

3.10. FT-Raman

Figure 10 shows the laser FT-Raman spectra of a reduced (H_2, 250°C) $YBa_2Cu_3O_7$ sample exposed to a mixture of CO_2 and H_2 at various temperatures. At 200 and 250°C, the vibration bands at 2870, 2940, and 2970 cm^{-1} attributable to CH_x, at 2574 cm^{-1} ascribed to formate and at 1900 cm^{-1} ascribed to C=O (58b, 66) were obviously detected. With the increase of adsorption temperature, these bands decreased in intensity and almost disappeared at 500°C. The CH_x bands were hard to be detected above 300°C. Bands at ca. 2300 cm^{-1} attributable to adsorbed CO_2 and weak bands at ca. 2100 cm^{-1} attributable to linear adsorbed CO were detected and their intensities decreased with temperature rise. These indicate that the hydrogenation of adsorbed CO_2 to produce species containing C, H, and O atoms is unlikely to occur at high temperatures.

4. DISCUSSION

4.1. Composition and Active Phase of Catalyst

The orthorhombic $YBa_2Cu_3O_7$ and tetragonal $YBa_2Cu_3O_6$ structures are shown in Fig. 11. They consist of an

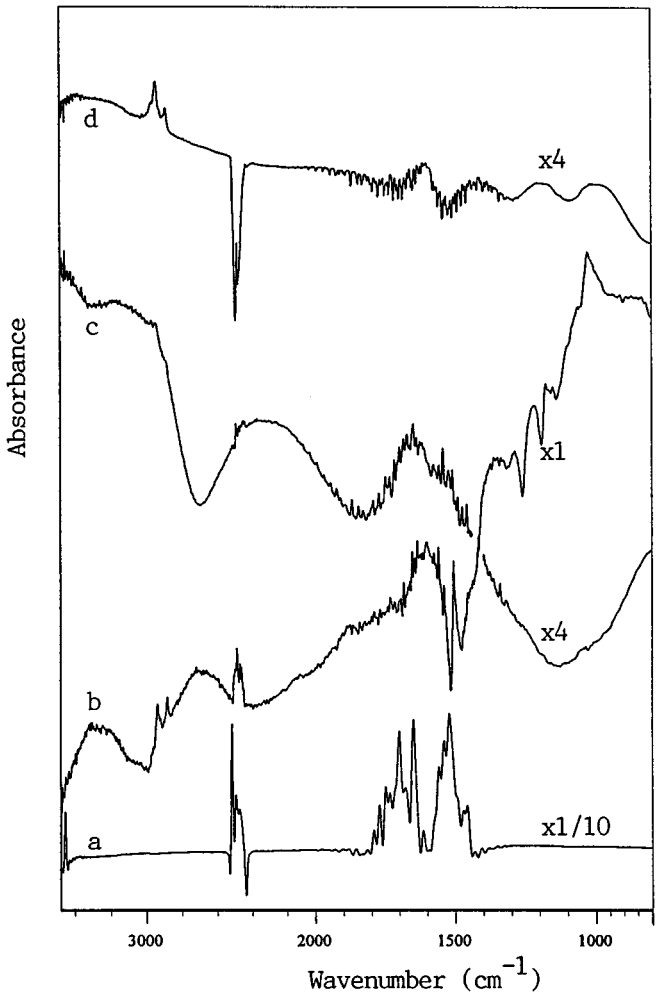

FIG. 9. Infrared spectra of (a) fresh $YBa_2Cu_3O_7$ exposed to H_2/CO_2 (3:1, 3.0 MPa) at 250°C (spectrum was referenced to that of fresh $YBa_2Cu_3O_7$); reduced (H_2, 250°C) $YBa_2Cu_3O_7$ exposed to (b) CO_2 (3.0 MPa) at 250°C, (c) CO_2 (3.0 MPa) at 300°C, and (d) H_2/CO_2 (3:1, 3.0 MPa) at 250°C (spectra were referenced to that of reduced (H_2, 250°C) $YBa_2Cu_3O_7$).

intergrowth sequence along the *c* axis:

$$|Cu(2)O_2\text{–}Y\text{–}Cu(2)O_2 \mid BaO\text{–}Cu(1)O_x\text{–}BaO|. \quad [8]$$

In the layers of $|Cu(2)O_2\text{–}Y\text{–}Cu(2)O_2|$, there are two CuO_2 sheets. In the layers of $|BaO\text{–}Cu(1)O_x\text{–}BaO|$, there is a variable oxygen content in CuO_x. The O_x is rather sensitive to the structures and physical properties of $YBa_2Cu_3O_7$. When x is close to 1, it is a superconductor with orthorhombic structure; when x is smaller than 0.5, it is an insulator with tetragonal structure. Under 1 atm of O_2, the upper limit of x in $YBa_2Cu_3O_{6+x}$ is about 0.96 (43). The Cu(2) in the CuO_2 sheets are five-fold coordinated in both the orthorhombic and the tetragonal structures. The Cu(1) in the CuO_x plane is four-fold coordinated in the orthorhombic structure and two-fold coordinated in the tetragonal structure. In tetragonal $YBa_2Cu_3O_6$, the *c* axis oxygen atoms are closer to the Cu(1) atoms in the CuO_x plane than to the Cu(2) atoms of a CuO_2 sheet. As x increases, the *c* axis oxygen moves away from the Cu(1) toward the Cu(2) atoms. In $YBa_2Cu_3O_{6+x}$, the content of oxygen (x) varies and the distribution of the formal oxidation states of copper atoms is controlled by the oxygen coordination at the Cu atoms. When the Cu(1) atoms are linearly coordinated by two oxygen atoms, as in the Cu(1) planes of the $YBa_2Cu_3O_6$ with tetragonal structure, the copper atoms bear a formal valence Cu^+. When the copper atoms are coordinated by five oxygen atoms, as in the $Cu(2)O_2$ sheets, the copper atoms may bear a formal valence $Cu^{(2+d)+}$, where $d=0$ in $YBa_2Cu_3O_6$ and $d=0.5$ in ideal $YBa_2Cu_3O_7$. Baetzold observed the localized small polarons of Cu^{3+} and O^- when studying the electronic defects of $YBa_2Cu_3O_7$ (67). The Cu(1) atoms coordinated by four coplanar oxygen atoms in the orthorhombic structure are in the valence of +2; whereas the Cu(1) atoms coordinated by two-fold oxygen atoms in the tetragonal structure are in the valence of +1. The oxygen atoms of the $Cu(1)O_x$ planes become mobile above 300°C (68). It is therefore feasible to remove oxygen progressively in the temperature interval $300 < T \leq 900$°C (69). It is possible to vary x in the $0 \leq x \leq 0.96$ range by changing the synthesis condition

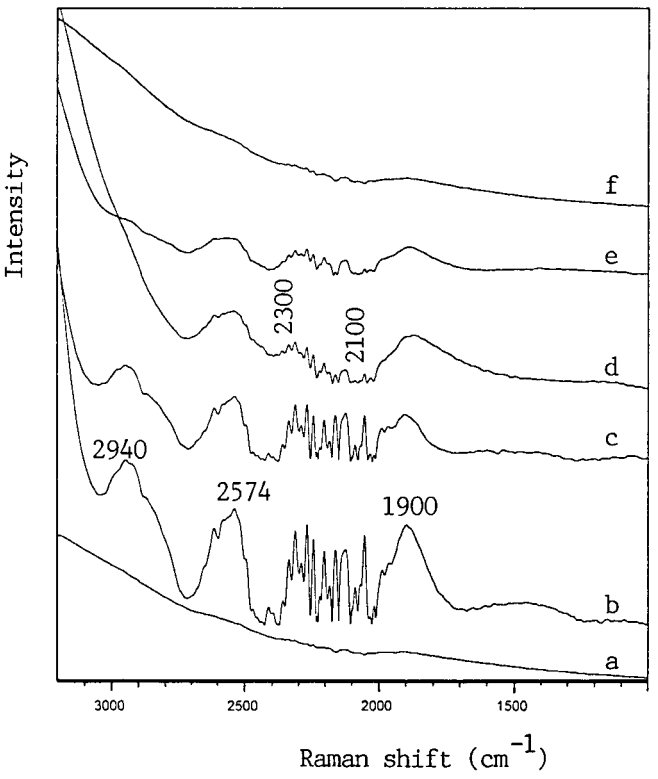

FIG. 10. FT-Raman spectra of reduced (H_2, 250°C) $YBa_2Cu_3O_7$ exposed to (a) N_2 at 250°C, (b) H_2/CO_2 (3:1) at 200°C, (c) H_2/CO_2 (3:1) at 250°C, (d) H_2/CO_2 (3:1) at 300°C, (e) H_2/CO_2 (3:1) at 400°C, and (f) H_2/CO_2 (3:1) at 500°C.

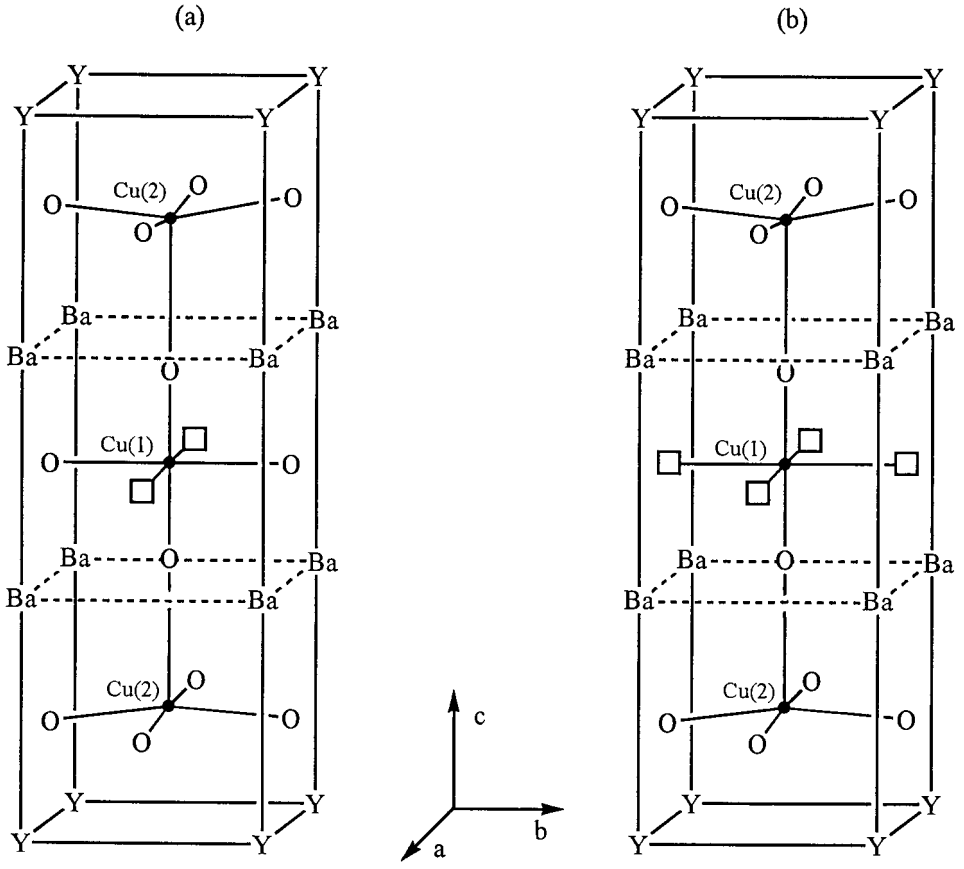

FIG. 11. Unit cell of (a) orthorhombic $YBa_2Cu_3O_7$ and (b) tetragonal $YBa_2Cu_3O_6$. Note: □ denotes an oxygen vacancy with a trapped electron.

(70). Cava *et al.* (71) reported that there were $O–Cu^+–O$ entities in $YCuO_2$.

A reduced $YBa_2Cu_3O_7$ sample with tetragonal phase showed activity in CO_2 hydrogenation whereas a fresh one with orthorhombic phase did not. It indicated that the tetragonal phase is suitable for CO_2 hydrogenation. H_2-TG/DTA results (Fig. 1A) illustrated that, after reduction at 250°C, $YBa_2Cu_3O_7$ has an average composition of $YBa_2Cu_3O_{6.325}$. The density of oxygen vacancies in the CuO_x plane of $YBa_2Cu_3O_{6.325}$ is less than that in a typical tetragonal structure of $YBa_2Cu_3O_6$. In other words, one can say that the number of coordinated oxygens is a little bit more than 2 in the CuO_x plane of $YBa_2Cu_3O_{6.325}$. In the orthorhombic structure of $YBa_2Cu_3O_7$, Cu^{2+} and Cu^{3+} co-exist; part of the Cu in the CuO_x layer is five-fold coordinated. In the tetragonal structure of $YBa_2Cu_3O_6$, Cu^+ and Cu^{2+} co-exist; most of the Cu(1) in the CuO_x layer is two-fold coordinated. When $YBa_2Cu_3O_7$ was reduced at 250°C, it changed to $YBa_2Cu_3O_{6.325}$, in which Cu^{2+} and Cu^+ co-exist; the Cu(1) in the CuO_x layer is two- and/or three-fold coordinated. So far, there is no evidence to support that Cu^0 can exist in a tetragonal structure of $YBa_2Cu_3O_6$. N_2O titration results suggested that there is no detectable metallic copper in tetragonal $YBa_2Cu_3O_{6.325}$. A $YBa_2Cu_3O_{6.325}$ sample exposed to N_2O at 90°C showed no change in EPR feature as compared to that of pure $YBa_2Cu_3O_{6.325}$. The XPS spectra (Fig. 3b) illustrated that after H_2-reduction at 250°C, the concentration of Cu^{2+} decreased. X-ray-induced Auger examination confirmed that Cu^+, rather than Cu^0, existed in the $YBa_2Cu_3O_{6.325}$ sample. When NO was adsorbed on $YBa_2Cu_3O_{6.325}$, there was a $NO–Cu^+$ EPR signal (Fig. 2j). All these phenomena indicate that there were Cu^+ ions but very little Cu^0 in $YBa_2Cu_3O_{6.325}$. Rojas *et al.* (72, 73) demonstrated that the Cu^{2+} ions placed in a perovskite lattice come to be reduced at temperatures much higher than that in massive CuO. In other words, the extent of Cu^{2+} reduction in $YBa_2Cu_3O_7$ is restricted. Brown-Bourzutschky *et al.* (74) reported that Cu^+ in $LaM_{1-x}Cu_xO_3$ (M = Cu, Ti) should be responsible for methanol synthesis from CO hydrogenation. The FTIR results in Fig. 8 indicated that the Cu–O–Cu bond stretching vibration has been modified after the reduction of $YBa_2Cu_3O_7$. When $YBa_2Cu_3O_7$ was reduced to $YBa_2Cu_3O_{6.325}$, the structure transformed from orthorhombic to tetragonal. In other words, the oxygen atoms in the *c* axis had moved away from Cu(2) and got closer to Cu(1), resulting in the small changes in FTIR (Fig. 8) features. The TPR profile (Fig. 1B(b)) showed that after H_2-reduction at 250°C, the $YBa_2Cu_3O_7$ sample still exhibited

H_2 consumption at 190°C, suggesting that the oxygen atoms in the CuO_x plane of $YBa_2Cu_3O_{6.325}$ were more mobile than those of the fresh $YBa_2Cu_3O_7$.

4.2. *Trapped Electrons and Oxygen Vacancies in Reduced $YBa_2Cu_3O_7$*

The EPR spectra in Figs. 2b and 2c show that by $YBa_2Cu_3O_7$ being heated at 800°C in He or being reduced at 250°C in H_2, trapped electrons were generated. As mentioned before, it is reported that the oxygen atoms in the CuO_x plane are mobile at temperatures above 300°C. Our O_2-TPD results (Fig. 4a) of fresh $YBa_2Cu_3O_7$ showed that O_2 desorption started at 600°C. In a helium atmosphere, if the sample was heated below 800°C, no EPR signal of trapped electrons was detected, indicating that only above 800°C, the *b* axis oxygen in the CuO_x plane could be removed significantly from the lattice. Thus, electron and oxygen vacancies would be generated along the *b* axis (see reaction [2] and Fig. 11). No significant oxygen desorption had been detected in the O_2-TPD profile of reduced $YBa_2Cu_3O_7$ (Fig. 4b), indicating that the oxygen atoms in the CuO_2 sheet are more stable than those in the CuO_x plane. Oxygen in the *b* axis can be removed in H_2-reduction at lower temperatures, resulting in the generation of trapped electrons and oxygen vacancies according to reactions [3] and [4]. The electrons trapped at oxygen vacancies formed F centers. Thus, the sequence [8] in $YBa_2Cu_3O_{6.325}$ can be written as

$$|CuO_2\text{–}Y\text{–}CuO_2 \mid BaO\text{–}Cu\text{–}[e^-]\text{–}BaO|. \qquad [9]$$

4.3. *Surface Redox Properties of $YBa_2Cu_3O_7$*

The catalytic behaviours of perovskite-type oxides (ABO_3) are closely related to the redox abilities of the *B* site ions. EPR results (Fig. 2c) demonstrated that the typical signal of Cu^{2+} ions dramatically decreased in intensity and the e^- signal was generated after H_2 reduction at 250°C. XPS studies (Fig. 3b) showed that, after reduction, there were large reductions in the intensities of the Cu^{2+} peak at 933.9 eV and the corresponding satellite peak at 943.0 eV. The H_2-TG/DTA measurements (Fig. 1A) showed that, after reduction, the composition of the catalyst should be $YBa_2Cu_3O_{6.325}$. All these pieces of evidence support the theory that Cu^{2+} ions in a $YBa_2Cu_3O_7$ sample could be reduced to a certain extent. After adsorption of CO_2 on $YBa_2Cu_3O_{6.325}$ at 250°C, the XPS results (Fig. 3e) illustrate that Cu^{2+} increased in concentration; the EPR results (Figs. 2d and 2e) show that the e^- signal disappeared. The TPR profile of a $YBa_2Cu_3O_7$ sample used in CO_2 hydrogenation (Fig. 1B(c)) shows a H_2 consumption peak at 280°C. These are clear pieces of evidence to suggest that CO_2 can oxidize the Cu^+ in the CuO_x plane of $YBa_2Cu_3O_{6.325}$ to Cu^{2+}. The results suggest that redox reactions such as reactions [5] and [6] had occurred. The EPR studies of CO_2/H_2 interaction with $YBa_2Cu_3O_{6.325}$ (Figs. 2f–2i) denote that no matter in a H_2-rich or CO_2-rich environment, there was no signal of trapped electrons. It suggests that, under the CO_2 hydrogenation conditions, CO_2 can take up a trapped electron and oxidize Cu^+ to Cu^{2+}.

4.4. *CO_2 Adsorption and Reaction with Reduced $YBa_2Cu_3O_7$*

The CO_2-TPD results shown in Fig. 5B indicate that there was one type of basic site on the surface of a reduced $YBa_2Cu_3O_7$ sample. We assume that the basic centers are the $[e^-]$ sites generated in H_2 reduction. The results in Figs. 5A and 5B and the FTIR spectra on CO_2 adsorption (Figs. 9a and 9b) also provide pieces of evidence that, after the reduction of $YBa_2Cu_3O_7$, the quantity of carbonates decreased, implying that the presence of trapped electrons and oxygen vacancies can hinder the formation of carbonates. FTIR (Fig. 9b) demonstrate that CO_2^-, rather than CO, was formed during CO_2 adsorption on reduced $YBa_2Cu_3O_7$ at low temperature, indicating that CO_2 takes up a trapped electron and generates CO_2^-. Considering the geometric and electronic effects, it is possible that CO_2 adsorption occurred on the oxygen vacancies in the CuO_x plane of reduced $YBa_2Cu_3O_7$. The oxygen atoms in CO_2 incorporated into the oxygen vacancies and took up a trapped electron, resulting in further oxidation of Cu^+ to Cu^{2+} (see reactions [6] and [7]). In the FTIR spectrum of CO_2 adsorption on reduced $YBa_2Cu_3O_7$ (Fig. 9b), in addition to the CO_2^-, CO_3, and HCO_3 bands, there are bands corresponding to the HCOO and H_2COO groups, indicating that formate and methylenebisoxy species were generated in the interaction of CO_2^- with surface hydrogen.

4.5. *H_2 Reaction with CO_2 Adspecies on Reduced $YBa_2Cu_3O_7$*

The TPSR results in Fig. 6 reveal that there were little CO_2 desorptions at 80, 150, 200, 330, and 650°C, indicating that the adsorbed CO_2 had been converted to carbonate or bicarbonate which decomposed to give CO_2 and H_2O. FT-Raman spectra (Fig. 10) support the theory that the co-adsorption of CO_2 and H_2 would result in the generation of CH, CH_2, and CH_3 groups. Above 600°C, CO desorption was observed, indicating that the RWGS reaction occurred at high temperatures. The *in situ*-FTIR spectrum (Fig. 9d) illustrates that, after the adsorptions of H_2 and CO_2, the bands of OH, HCOO, H_2COO, CH_2O, HCO, CH_3O, and CH_3OCHO appeared, whereas compared to those of Fig. 9b, the intensities of the H_2COO bands were weakened. The results indicate that the adsorbed hydrogen had reacted with H_2COO; methanol and dimethyl ether were generated via the CH_2O and HCO intermediates.

The results of pulsing CO_2 in a H_2 flow (Fig. 7) at 250°C show that there was one CO_2 response peak for each pulse.

In the initial CO_2 pulses, no peaks with $m/z = 44$ were detected, implying that, in the presence of hydrogen, CO_2 adsorbed rather strongly on the catalyst. During CO_2 pulsing in H_2, we trapped methoxy and formate. Both the FTIR and CD_3I-trapping results imply that, in the presence of H_2, (i) CO_2 adsorbs strongly on reduced $YBa_2Cu_3O_7$; (ii) H_2COO species can be transformed to other species; and (iii) HCOO is readily generated. The reaction between adsorbed hydrogen and CO_2 could be depicted as

$$H + HCOO \rightarrow H_2COO, \quad [10]$$

$$H_2COO + H \rightarrow HCO + H_2O, \quad [11]$$

$$HCO + 2H \rightarrow H_3CO. \quad [12]$$

The H_2COO species is unstable and transformed easily to other intermediates such as formyl and methoxy in the presence of hydrogen. At higher temperatures, the formyl could be decomposed to CO. The fact that the absorbance band of methylenebisoxy was relatively weak in Fig. 9d supports the above speculation.

4.6. Hydrogen Adsorption and Spillover on $YBa_2Cu_3O_7$

Previous work by Fujita *et al.* on a Cu/SiO_2 catalyst has shown that H_2 adsorbs dissociatively on copper with an adsorption heat of about 12 kcal mol^{-1} and an activation barrier of about 10.5 kcal mol^{-1} (75). Other studies on Cu/ZrO_2 catalysts suggest that Cu is more effective than ZrO_2 in dissociating H_2, and Cu serves to adsorb H_2 dissociatively and to provide a source of atomic hydrogen (76–78). For $YBa_2Cu_3O_7$, H_2 may adsorb preferably on the Cu^+ sites of CuO_x, offering electrons to oxygen vacancies to form F centers, into which the oxygen atoms of CO_2 insert. The generation of HCOO, HCOOH, and H_2COO is due to the interaction between the adsorbed H and adsorbed CO_2 by means of H spillover. Fisher *et al.* proposed a methanol synthesis mechanism of CO_2 hydrogenation on $Cu/ZrO_2/SiO_2$, in which Cu and Zr are envisioned to be in close proximity (33). The H adsorbed on Cu can spill over to the carbonate on Zr to form HCOO and H_2COO intermediates, leading finally to the production of methanol. In the CuO_x plane of reduced $YBa_2Cu_3O_7$, if H_2 adsorbed on the Cu site and CO_2 adsorbed on the oxygen vacancies, there would be no blockage between the two. So the spillover of H to CO_2 to generate COOH and COHOH intermediates could be feasible. The COOH and COHOH species could rearrange to relatively more stable species, such as HCOO (formate) and H_2COO (methylenebisoxy). Due to H spillover from Cu^+, HCOO and H_2COO species could transform to HCOOH, HCOHOH, H_2COOH, and H_2COHOH. The HCOHOH and H_2COHOH intermediates could dehydrate to produce HCO (formyl) and H_2CO (formaldehyde), which could be hydrogenated to H_3CO (methoxide). In addition, the FT-Raman spectra (Fig. 10) illustrate that CH_x ($x = 1$, 2, and 3) species were generated at 200 and 250°C, implying that the spillover of hydrogen proceeds rather efficiently.

4.7. Reaction Intermediates of CO_2 Hydrogenation on $YBa_2Cu_3O_7$

Over copper catalysts, CO hydrogenation to methanol is known to occur via a formyl (CHO) intermediate, whereas the CO_2 hydrogenation to methanol involves a formate (HCOO) intermediate (79, 80). Clarke *et al.* suggested that methanol is formed via the stepwise hydrogenation of HCOO–Cu to methylenebisoxy, and the methoxide species is the final precursor to methanol on a Cu/SiO_2 catalyst (81). With the adsorption of CO_2 on reduced $YBa_2Cu_3O_7$, bands of formate and methylenebisoxy were observed at 250°C (Fig. 9b). At 350°C, the formate bands almost disappeared and that of methylenebisoxy vanished, whereas the CO band appeared (Fig. 9c). It means that the intermediates, especially methylenebisoxy, are unstable at high temperatures. In other words, high temperatures are suitable for CO formation. The FT-Raman spectra in Fig. 10 illustrate that high temperature is unfavourable to the C–H and C=O formation. After CO_2 and H_2 adsorptions at 250°C, the FTIR bands of formate, formyl, formaldehyde, methoxide, and C–O–C appeared, but the band of methylenebisoxy was observed in low intensity (Fig. 9d). It indicates that, with more hydrogen spilled over to methylenebisoxy, the intermediate rearranged and decomposed.

4.8. Possible Reaction Mechanism for CO_2 Hydrogenation to Methanol on $YBa_2Cu_3O_7$

Based on the preceding arguments, a possible mechanism for CO_2 hydrogenation to methanol on reduced $YBa_2Cu_3O_7$ is presented in Fig. 12. In this scheme, H_2 and CO_2 adsorbed on Cu^+ and oxygen vacancies (with trapped electrons), respectively. The spillover of H from Cu^+ to the adsorbed CO_2 would lead to the formation of HCOO, HCOHOH, H_2COO, H_2COOH, and H_2COHOH. The dehydration of HCOHOH and H_2COHOH would give HCO (formyl) and H_2CO (formaldehyde), respectively, which reacts with H to produce methanol.

4.9. Catalytic Performance Interpretation

Tables 1–3 indicate that high pressure, high space velocity, and low temperature are favourable to methanol synthesis. The by-products of methanol synthesis are CO and CH_3OCH_3. In the FTIR spectra of CO_2 adsorption at 250°C (Fig. 9b), one cannot observe any band due to adsorbed CO on Cu, indicating that the dissociation of CO_2 to CO and O on $YBa_2Cu_3O_7$ is difficult. The dehydrogenation of H_2CO and HCO in the CO_2 hydrogenation scheme (Fig. 12) may be responsible for the formation of CO. High pressure, low temperature, and high space velocity probably can suppress

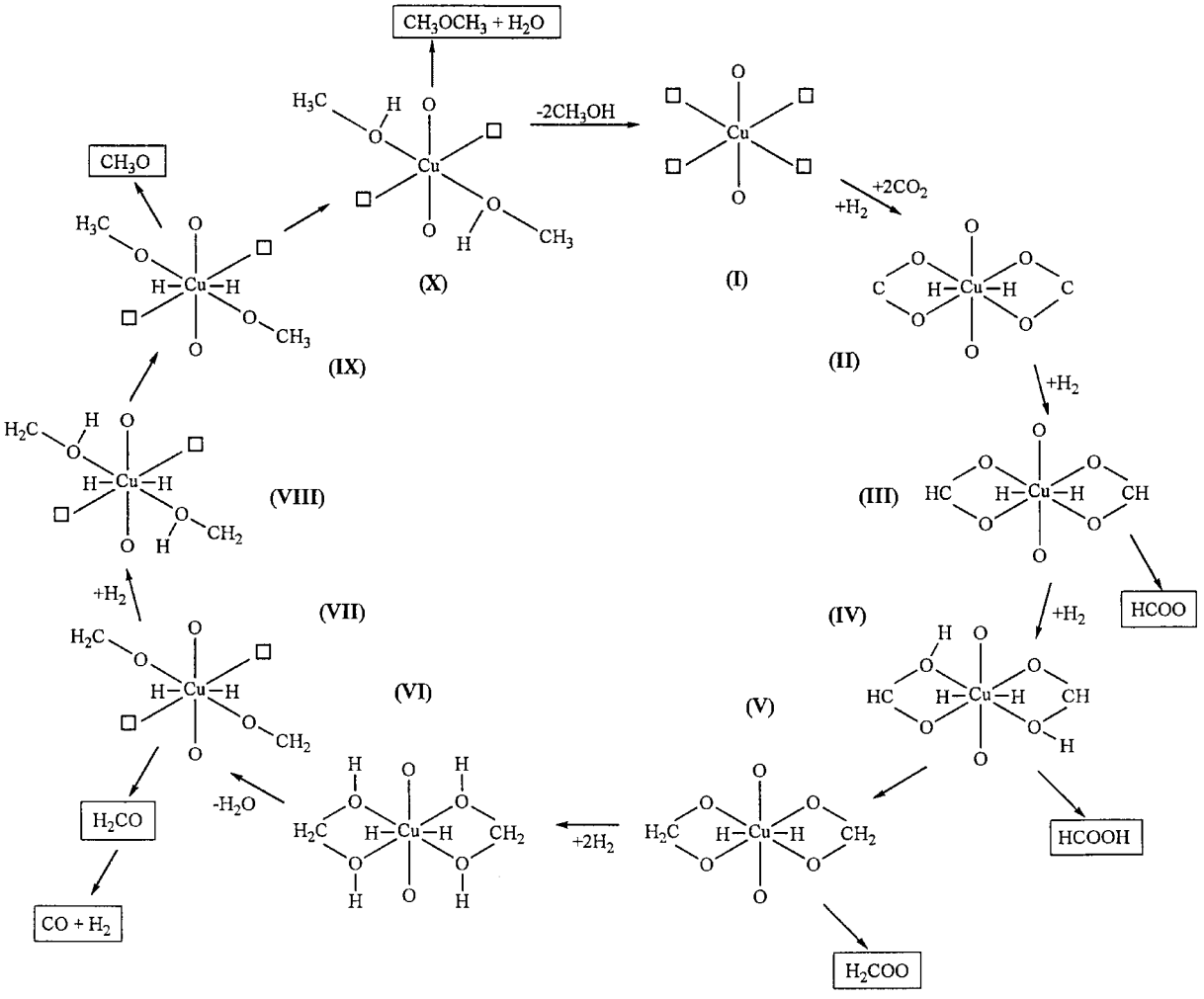

FIG. 12. Proposed mechanism for the synthesis of methanol from CO_2 and H_2 over tetragonal $YBa_2Cu_3O_6$.

the dehydrogenation of CH_2O and HCO. Low temperature is suitable for hydrogen spillover to generate CH_x ($x = 1$, 2, and 3) functional groups for methanol production. The effect of reaction conditions on CH_3OCH_3 production is similar to that on CH_3OH, implying that both CH_3OCH_3 and CH_3OH are generated from the same intermediates. The CO_2/H_2 adsorption FTIR spectrum (Fig. 9d) exhibits a band of C–O–C stretching. Hence, CH_3OCH_3 may be formed from two CH_3OH via a dehydration step on the surface of reduced $YBa_2Cu_3O_7$.

5. CONCLUSIONS

$YBa_2Cu_3O_7$ H_2-reduced at 250°C was active for methanol synthesis via CO_2 hydrogenation. After reduction, the structure of $YBa_2Cu_3O_7$ transformed from orthorhombic to tetragonal. The composition of the tetragonal structure is $YBa_2Cu_3O_{6.325}$ in which Cu^{2+} and Cu^{+} co-exist with no metallic Cu^0. In $YBa_2Cu_3O_{6.325}$, there are trapped electrons and oxygen vacancies. CO_2 adsorbed on $YBa_2Cu_3O_{6.325}$ could take up the trapped electrons, resulting in the oxidation of Cu^{+} to Cu^{2+}. Therefore, the redox between Cu^{+} and Cu^{2+} might play an important role in CO_2 hydrogenation. The intermediates of CO_2 hydrogenation were HCOO, H_2COO, HCO, and H_2CO species. We have proposed a mechanism for CO_2 hydrogenation on $YBa_2Cu_3O_{6.325}$ in which H_2 is dissociatively adsorbed on the Cu^{+} site and CO_2 is adsorbed on the oxygen vacancies via its two oxygen atoms. The adsorbed CO_2 then undergoes stepwise hydrogenation to COOH, COHOH, HCOOH, HCOHOH, and H_2COHOH with H being supplied by means of H spillover from Cu^{+}. The intermediates COOH, COHOH, HCOHOH, and H_2COHOH could transform to formate, methylenebisoxy, formyl, and formaldehyde groups, respectively. The final and crucial step in this sequence would be the hydrogenation of formyl and formaldehyde. The dehydrogenation of formyl and formaldehyde can produce CO, a major by-product in methanol synthesis.

ACKNOWLEDGMENT

The work described above was fully supported by a grant from the Research Grants Council of the Hong Kong Special Administration Region, China (Project RGC/96-97/02).

REFERENCES

1. Kagan, Y. B., Liberov, L. G., Slivinskii, E. V., Loktev, S. M., Lin, G. T., Rozovskii, A. Y., and Bashkirov, A. N., *Dokl. Akad. Nauk. SSSR* **221**, 1093 (1975).
2. Rozovskii, A. Y., Lin, G. T., Liberov, L. G., Slivinskii, E. V., Loktev, S. M., Kagan, Y. B., and Bashkirov, A. N., *Kinet. Katal.* **18**, 691 (1977).
3. Rozovskii, A. Y., *Russ. Chem. Rev.* **58**, 41 (1987); *Kinet. Katal.* **21**, 97 (1980).
4. Chinchen, G. C., Denny, P. J., Parker, D. J., Spenser, M. S., and Whan, D. A., *Appl. Catal.* **30**, 333 (1987).
5. Chinchen, G. C., Mansfield, K., and Spenser, M. S., *CHEMTECH* **20**, 692 (1990).
6. Chanchlani, K. G., Hudgins, P. R., and Silveston, P. L., *J. Catal.* **136**, 59 (1992).
7. Sahibzada, M., Metcalfe, I. S., and Chadwick, D., *J. Catal.* **174**, 111 (1998).
8. Liu, G., Willcox, D., Garland, M., and Kung, H. H., *J. Catal.* **90**, 139 (1984).
9. Denise, B., Sneeden, R. P. A., and Hamon, C., *J. Mol. Catal.* **17**, 339 (1982).
10. Takegawa, M., and Ohsugi, M., *J. Catal.* **107**, 161 (1987).
11. Lee, J. S., Lee, K. H., Lee, S. Y., and Kim, Y. G., *J. Catal.* **144**, 414 (1993).
12. Klier, K., Chatikavanj, V., Herman, R. G., and Simmons, G. W., *J. Catal.* **74**, 343 (1982).
13. Vedage, G. A., Pitchai, R., Herman, R. G., and Klier, K., "Proceedings, 8th International Congress on Catalysis, Berlin, 1984," Vol. II, p. 47. Dechema, Frankfurt-am-Main, 1984.
14. Chinchen, G. C., Waugh, K. C., and Whan, D. A., *Appl. Catal.* **25**, 101 (1986).
15. Robbins, J. L., Iglesia, E., Kelkar, C. P., and DeRites, B., *Catal. Lett.* **10**, 1 (1991).
16. Klier, K., *Adv. Catal.* **31**, 243 (1982).
17. Nonneman, L. E. Y., and Ponec, V., *Catal. Lett.* **7**, 213 (1990).
18. Okamoto, Y., Fukino, K., Imanaka, T., and Eranishi, S., *J. Chem. Soc., Chem. Commun.* 1405 (1982); *J. Phys. Chem.* **87**, 3747 (1983).
19. Frost, J. C., *Nature* **334**, 577 (1988).
20. Rostrup-Nielsen, J. R., and Nielsen, H., "Deactivation and Poisoning of Catalysis" (J. Oudar and H. Wise, Eds.), p. 259. Dekker, New York, 1985.
21. Clausen, B. S., Steffensen, G., Fabius, B., Villadsen, J., Feidenhans'l, R., and Topsøe, H., *J. Catal.* **132**, 524 (1991).
22. Clausen, B. S., Schiøtz, J., Gråbæk, L., Ovesen, C. V., Jacobsen, K. W., Nøskov, J. K., and Topsøe, H., *Topics Catal.* **1**, 367 (1994).
23. Clausen, B. S., Gråbæk, L., Steffensen, G., Hansen, P. L., and Topsøe, H., *Catal. Lett.* **20**, 23 (1993).
24. Ovesen, C. V., Clausen, B. S., Schiøtz, J., Stoltze, P., Topsøe, H., and Nøskov, J. K., *J. Catal.* **168**, 133 (1997).
25. Chinchen, G. C., Spenser, M. S., Waugh, K. C., and Whan, D. A., *J. Chem. Soc., Faraday Trans. 1* **83**, 2193 (1987).
26. Chinchen, G. C., Waugh, K. C., and Whan, D. A., *Appl. Catal.* **25**, 101 (1986).
27. Torras, J., Ricart, J. M., Illas, F., and Rubio, J., *Surf. Sci.* **297**, 57 (1993).
28. Bagus, P. S., and Illas, F., *Phys. Rev. B* **42**, 10852 (1990).
29. Muhler, M., Törnqvist, E., Nielsen, L. P., and Clausen, B. S., *Catal. Lett.* **25**, 1 (1994).
30. Burch, R., Golunski, S. E., and Millar, G. J., *Catal. Lett.* **5**, 55 (1990).
31. Bowker, M., Hadden, R. A., Houghton, H., Hyland, J. N., and Waugh, K. C., *J. Catal.* **109**, 263 (1988).
32. Bowker, M., and Madix, R. J., *Surf. Sci.* **102**, 542 (1981).
33. Fisher, I. A., and Bell, A. T., *J. Catal.* **172**, 222 (1997).
34. Hayden, B. E., Prince, K., Woodruff, D. P., and Bradshaw, A. M., *Surf. Sci.* **133**, 589 (1983).
35. Newsome, D. S., *Catal. Rev. Sci. Eng.* **21**, 275 (1980), and references therein.
36. Waches, J. E., and Madix, R. J., *J. Catal.* **53**, 208 (1978).
37. Gür, T. M., Wise, H., and Huggins, R. A., *Catal. Lett.* **23**, 387 (1994).
38. Hansen, S., Otamiri, J., Bovin, J. O., and Andersen, A., *Nature* **334**, 143 (1988).
39. Tabata, K., Fukui, H., Kohiki, S., Mizuno, N., and Misono, M., *Chem. Lett* **799** (1988).
40. Mizuno, N., Yamato, M., and Misono, M., *J. Chem. Soc., Chem. Commun.* **887** (1988).
41. Maeno, Y., Tomita, T., Kyogoku, M., Awaji, S., Aoki, Y., Hosino, K., and Fujita, T., *Nature* **328**, 512 (1987).
42. Islam, M. S., and Baetzold, R. C., *Phys. Rev. B* **40**, 10926 (1989).
43. Goodenough, J. B., and Manthiram, A., *J. Solid State Chem.* **88**, 115 (1990).
44. Dandekar, A., and Vannice, M. A., *J. Catal.* **178**, 621 (1988).
45. Schalten, J. J. F., and Konvalinka, J. A., *J. Chem. Soc., Faraday Trans.* **65**, 2465 (1969).
46. Arias, A. M., Cataluña, R., Conesa, J. C., and Soria, J., *J. Phys. Chem. B* **102**, 809 (1998).
47. Chao, C. C., and Lunsford, J. H., *J. Chem. Phys.* **57**, 2890 (1972).
48. Millar, G. J., and Rochester, C. H., *Topics Catal.* **3**, 103 (1996).
49. Solymosi, F., and Knözinger, H., *J. Catal.* **122**, 166 (1990).
50. Kasai, P. H., and McLeod, D., *J. Chem. Phys.* **55**, 1566 (1971).
51. Sojka, Z., Che, M., and Giamello, E., *J. Phys. Chem.* **97**, 305 (1997).
52. Chao, C. C., and Lunsford, J. H., *J. Phys. Chem.* **76**, 1546 (1972).
53. Arakawa, T., and Adachi, G., *Mater. Res. Bull.* **24**, 529 (1989).
54. D'Huysser, A., Wrobel, G., and Bonnelle, J. P., *Nouv. J. Chim.* **6**, 437 (1982).
55. D'Huysser, A., Le Calonnec, D., Lenglet, M., Bonnelle, J. P., and Jørgensen, C. K., *Mater. Res. Bull.* **19**, 1157 (1984).
56. Okamoto, Y., Fukono, K., Imanaka, T., and Teranishi, S., *J. Phys. Chem. B* **87**, 3747 (1983).
57. Somorjai, G. A., "Chemistry in Two Dimensions Surfaces." Cornel University Press, Ithaca, NY, 1981.
58. Schrader, B., "Infrared and Raman Spectroscopy," (a) pp. 401–407, (b) pp. 190, 209, 212. VCH Verlagsgesellschaft mbH/VCH, Weinheim New York, 1995.
59. Edwards, J. F., and Schrader, J. L., *J. Phys. Chem.* **88**, 5620 (1984).
60. Hertl, W., *Langmuir* **5**, 96 (1989).
61. Millar, G. J., Rochester, C. H., and Waugh, K. C., *J. Chem. Soc., Faraday Trans.* **87**, 1491 (1991).
62. Stuve, E. M., Madix, R. J., and Sexton, B. A., *Surf. Sci.* **119**, 279 (1982).
63. Clarke, D. B., Lee, D. K., Sandoval, M. J., and Bell, A. T., *J. Catal.* **142**, 27 (1993).
64. Monti, D. M., Cant, N. W., Trimm, D. L., and Wainwright, M. S., *J. Catal.* **100**, 17 (1986).
65. Millar, G. J., Rochester, C. H., and Waugh, K. C., *J. Chem. Soc., Faraday Trans.* **81**, 2785 (1991).
66. Bellamy, L. J., "The Infrared Spectra of Complex Molecules," 3rd ed., Vol. 1, pp. 5–9, Chapman and Hall, London, 1986.
67. Baetzold, R. C., *Phys. Rev. B* **38**, 11304 (1988).
68. Manthiram, A., Swinnea, J. S., Sui, Z. T., Steinfink, H., and Goodenough, J. B., *J. Am. Chem. Soc.* **109**, 6667 (1987).
69. Manthiram, A., and Goodenough, J. B., *Nature* **329**, 701 (1987).
70. More, C., and Duran, P., "Properties and Applications of Perovskite-type Oxides" (L. G. Tejuca and J. L. G. Fierro, Eds.), p. 33. Marcel Dekker, Inc., New York, 1992.

71. Cava, R. J., Zandbergen, H. W., Ramirez, A. P., Takagi, H., Chen, C. T., Krajewski, J. J., Peck, W. F., Jr., Waszczak, J. V., Meigs, G., Roth, R. S., and Schneemeyer, L. F., *J. Solid State Chem.* **104**, 437 (1993).
72. Rojas, M. L., Fierro, J. L. G., Tejuca, L. G., and Bell, A. T., *J. Catal.* **124**, 41 (1990).
73. Rojas, M. L., Fierro, J. L. G., and Tejuca, L. G., *J. Solid State Chem.* **89**, 299 (1990).
74. Brown-Bourzutschky, J. A., Homs, N., and Bell, A. T., *J. Catal.* **124**, 52 (1990).
75. Fujita, S., Usui, M., Ito, H., and Takezawa, N., *J. Catal.* **157**, 403 (1995).
76. Fisher, I. A., Woo, H. C., and Bell, A. T., *Catal. Lett.* **44**, 11 (1997).
77. Burch, R., Golunski, S. E., and Spencer, M. S., *J. Chem. Soc., Faraday Trans.* **86**, 2683 (1990).
78. He, M. Y., and Ekerdt, J. G., *J. Catal.* **90**, 17 (1984).
79. Bart, J. C. J., and Sneeden, R. P. A., *Catal. Today* **2**, 1 (1987).
80. Tagawa, T., Pleizier, G., and Amenomiya, Y., *Appl. Catal.* **18**, 285 (1985).
81. Clarke, D. B., and Bell, A. T., *J. Catal.* **154**, 314 (1995).